ISSN 0030-400X, Optics and Spectroscopy, 2020, Vol. 128, No. 8, pp. 1118–1124. © Pleiades Publishing, Ltd., 2020.
Russian Text © The Author(s), 2020, published in Optika i Spektroskopiya, 2020, Vol. 128, No. 8, pp. 1108–1114.

SPECTROSCOPY
OF CONDENSED MATTER

Specific Features of Photoluminescence of $CH_3NH_3PBI_3$ Perovskites Synthesized on Nanostructured TiO_2 Surface

D. A. Afanasyev[a], * and N. Kh. Ibrayev[a]

[a] *Institute of Molecular Nanophotonics, Buketov Karaganda State University, Karaganda, 100028 Republic of Kazakhstan*

**e-mail: a_d_afanasyev@mail.ru*

Received February 25, 2020; revised February 25, 2020; accepted April 15, 2020

Abstract—The influence of nanostructured titania surface on the photoluminescence of organometallic perovskite $CH_3NH_3PbI_3$ films is studied. It is found that the $CH_3NH_3PbI_3$ luminescence intensity and lifetime decrease on the TiO_2 surface, which testifies to charge transfer from perovskite to titania. Charge transfer occurs most efficiently for perovskite films synthesized on the surface of mesoporous TiO_2 films. The time dependence of magnetic effect on the luminescence of $CH_3NH_3PbI_3$ on mesoporous TiO_2 films is related to the recombination luminescence caused by forward and backward electron transfer between perovskite and titania.

Keywords: titania, perovskite, nanostructured films, luminescence kinetics, magnetic effect

DOI: 10.1134/S0030400X20080032

INTRODUCTION

Investigations in the field of application of organic materials for fabrication of solar-to-electric energy converters led to the development of two new types of solar cells, namely, dye-sensitized solar cells (DSSCs) and polymer solar cells [1, 2]. Work [3] performed in 2009 and aimed at improvement of DSSCs resulted in the creation of perovskite solar cells (PSCs). These cells are based on organo-inorganic compounds with composition $MaPbX_3$, where Ma is methylammonium and X is a halogen (Br, I, or Cl). For the period from 2009 to 2020, the efficiency of PSCs increased from 3.8 to 25% [4].

The specific features of charge transfer in PSCs are studied by laser kinetic spectroscopy methods. These methods make it possible to estimate lifetimes of charge carriers, determine the efficiency of charge transfer from the perovskite film to semiconductor layers with *n*- and *p*-type conductivity, and determine the concentration of defects in perovskite films [5, 6]. Despite the results achieved, some questions still need more detailed studies. One of these questions is the effect of the spin state of charge carriers on the light-to-electric energy conversion efficiency in PSCs.

Perovskites have a strong spin–orbit coupling caused by the presence of heavy atoms (Pb, I), which considerably affects the spin–lattice relaxation time for spin-correlated electron–hole pairs. In this case, a change in the spin–orbit coupling value leads to a change in the PSC efficiency [7]. Some well-developed and widely used methods for studying the spin state of free charge carriers and charge-transfer complexes are based on the influence of an external magnetic field (MF) on the photocurrent and the intensity of photo- and electroluminescence [8]. These methods allow one to determine the specific features of the effect of an external MF at the stages of formation, transport, or recombination of charge carriers in semiconductor materials. It is agreed that the first study of the influence of an external MF on photocurrent, electroluminescence, and photoluminescence is work [9]. The authors of this work studied the influence of an external MF on photoluminescence intensity in the case of circularly polarized laser excitation and determined the mechanism of the effect of an external MF on photoprocesses in perovskite films, i.e., Δg mechanism. The value of Δg factor for electron–hole pairs in $MaPbI_3$ was measured to be $\Delta g \sim 0.65$.

Using first principle quantum-chemical calculations based on the Rashba spin–orbit model, the authors of [10] showed that the recombination rate of charge carriers in $MaPbI_3$ decreases due to the spin-forbidden transition. This, in turn, increases the light-to-electric energy conversion efficiency in perovskites. These results are important both for understanding the mechanisms of photoprocesses in organometallic halide perovskites and for optimization of the design of PSCs.

Continuation of the studies aimed at the influence of an external MF on photoprocesses in PSCs allowed one to determine the effect of the substrate and treatment conditions on the properties of perovskite films [7]. The *g*-factors of excitons and charge carriers, spin relaxation times, and hyperfine interactions of charge

carriers and nuclear spins were measured in [11] based on time-resolved spectroscopy. In addition, a promising method for determining the mobility and concentration of both majority and minority charge carriers, recombination time, diffusion length, and recombination coefficient is the measurement of the Hall effect upon photoexcitation of samples [12].

The study of the luminescence kinetics of perovskite films in an MF will provide additional information about processes of charge transfer through an oxide semiconductor–perovskite interface. In the present work, we report the results of investigation of the influence of the TiO_2 film surface morphology (compact and mesoporous) on charge-transfer processes in $CH_3NH_3PbI_3$ and on the time-dependent magnetic effect on the photoluminescence of perovskite films.

EXPERIMENTAL

As substrates for synthesis of $CH_3NH_3PbI_3$ films, we chose compact (TiO_2/C), rough (TiO_2/R), and mesoporous (TiO_2/M) films of titanium dioxide TiO_2. These films were formed on the surfaces of glass plates coated with a transparent electroconducting layer of fluorine-doped tin oxide (FTO) (Sigma-Aldrich). The compact TiO_2 layers were formed using a Ti-Nanoxide BL/SC solution (Solaronix). We used a method recommended by the manufacturer for fabrication of defect-free TiO_2/M films. To synthesize mesoporous films, we used a paste based on 20-nm TiO_2 anatase nanoparticles (Sigma-Aldrich) and ethylene glycol as a solvent. The paste was deposited on the substrate surface by spin coating. The TiO_2 concentration and the film deposition conditions were chosen so that the film thickness was minimal and the surface was uniform. The rough films were formed by hydrothermal synthesis in a hermetic autoclave for 24 h at a temperature of 120°C. The synthesis of samples with nanostructured TiO_2 surfaces and their properties are described in detail in [13]. The $CH_3NH_3PbI_3$ perovskite film was synthesized by a two-stage method according to work [14].

As a material with hole conductivity, we used Spiro-OMeTAD ($N^2,N^2,N^{2'},N^{2'},N^7,N^7,N^{7'},N^{7'}$-octakis(4-methoxyphenyl)-9,9'-spirobi[9H-fluorene]-2,2',7,7'-tetramine) films. Solutions of Spiro-OMeTAD in chlorobenzene with 4-tret-butyl-pyridine and bis(trifluoromethane) sulfonimide lithium salt additives were prepared. The films were formed by centrifuging according to the method described in detail in [14, 15].

The microstructural properties of the synthesized films were studied using a TESCAN Mira 3 scanning electron microscope. The absorption spectra of films were recorded using a Cary 300 (Agilent) spectrophotometer. The fluorescence spectra were measured on a Cary Eclipse (Agilent) spectrofluorimeter. The fast fluorescence kinetics of polymer films was measured on a pulsed spectrofluorimeter (Becker & Hickl) with a picosecond resolution and recording in the time-correlated photon counting mode. The fluorescence of samples was excited by a pulsed semiconductor laser with wavelength λ_{gen} = 488 nm and pulse duration (FWHM) τ = 120 ps. The influence of an external magnetic field on the luminescence intensity of perovskite films was studied according to the method described in [16].

RESULTS AND DISCUSSION

Figure 1 presents electron microscope images of the surfaces of (a) compact, (b) rough, and (c) mesoporous TiO_2 films. The compact TiO_2 film covers the substrate surface completely, without gaps. The TiO_2/C film in the substrate plane contains spherical and cylindrical structural elements. The diameter of the spherical particles is ~70 nm. The diameter of the cylindrical elements is also 70 nm, and the length varies from 100 to 500 nm. The rough TiO_2 film contains nanorods with an average diameter of 50 nm. The nanorods are oriented at different angles to the substrate surface. The TiO_2/R film thickness is ~600 nm. The mesoporous TiO_2 film is nonuniform in thickness and contains grains from 400 nm to 5 μm in size (Fig. 1c). These grains are agglomerates of titania nanoparticles (nanoparticle size 20 nm), from which the film was prepared. The film thickness is ~ 500 nm.

The images of surfaces of $MaPbI_3$ perovskite synthesized on the contact and mesoporous TiO_2 films are shown in Fig. 2. $MaPbI_3$ perovskite on the TiO_2/R surface is identical to the film on TiO_2/M. Comparison of the images presented in Figs. 1 and 2 shows that the synthesis of perovskite films occurs with formation of structures that considerably differ from the surface structure of TiO_2 films. A dense perovskite film with a characteristic grain size of ~1 μm is formed on the TiO_2/C surface (Fig. 2a). Perovskite films on the TiO_2/M surface have a crystalline structure with crystallite sizes of 100–200 nm (Fig. 2b). The crystallites are loosely distributed. The microstructure of the perovskite films on the TiO_2/R surface is identical to the structure of films formed on TiO_2/M.

Figure 3 shows the images of the cross section of a TiO_2/M–$MaPbI_3$ sample, which were obtained using secondary (SE) and backscattered (BSE) electron detectors. From these images, we determined the thickness of different layers (Table 1). The BSE image reveals the presence of three layers with different compositions. The lower layer 600 nm thick is the FTO layer. The intermediate, darker layer is TiO_2. Its thickness is ~260 nm. The upper, lighter layer corresponds to perovskite. The perovskite layer observed on the BSE image exhibits darker regions, which most probably belong to the mesoporous TiO_2 film. Thus, the

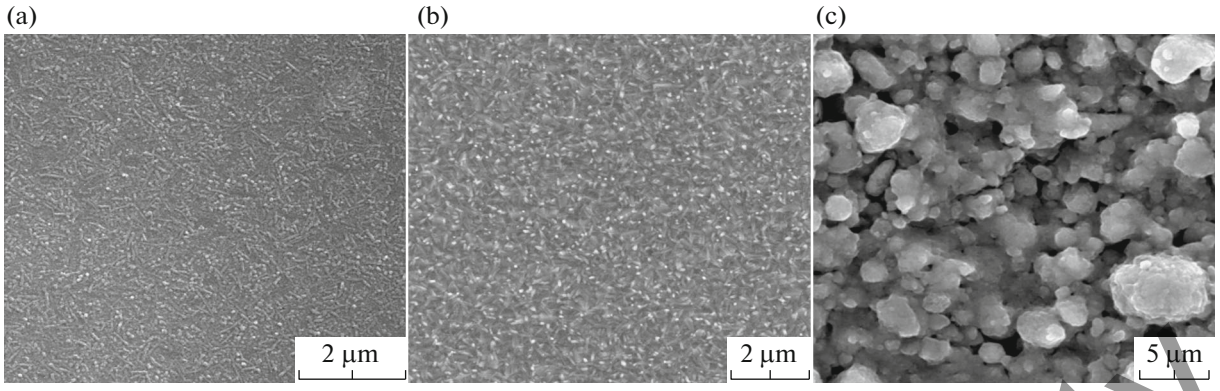

Fig. 1. Electron microscope images of the surfaces of (a) compact, (b) rough, and (c) mesoporous TiO_2 films.

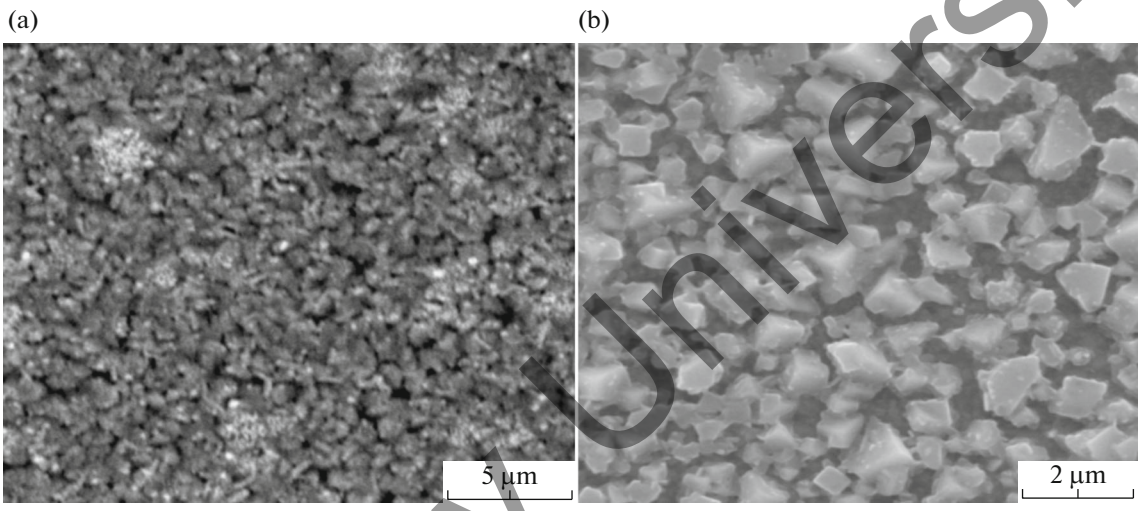

Fig. 2. Electron microscope images of $CH_3NH_3PbI_3$ perovskite films on surfaces of (a) compact and (b) mesoporous TiO_2 films.

TiO_2/M–$MaPbI_3$ structure consists of a three-layer film. The lower layer represents the mesoporous TiO_2 film. The upper layer is a $CH_3NH_3PbI_3$ film of uniform thickness (~600 nm). The intermediate layer between the TiO_2 and $MaPbI_3$ films consist of porous TiO_2 with a $MaPbI_3$ film formed in it.

The absorption and luminescence spectra were measured for perovskite films synthesized on the surfaces of TiO_2 films with different surface morphologies. The absorption spectra of $CH_3NH_3PbI_3$ films are shown in Fig. 4a. For comparison, Fig. 4a also shows the absorption spectra of a PbI_2 film (curve *5*). Analysis of the spectra shows that the absorption spectrum of the PbI_2 film differs from the absorption spectrum of the $CH_3NH_3PbI_3$ film. Thus, at the second stage, addition of CH_3NH_3I on the sample surface leads to the formation of the $CH_3NH_3PbI_3$ film. The luminescence spectra of the films are shown in Fig. 4b. The luminescence intensity maximum lies in the wavelength range from 740 to 765 nm, which corresponds to the data available in the literature [12, 14]. The luminescence intensity maximum of perovskite films shifts to shorter wavelengths in the series of surfaces FTO–TiO_2/C–TiO_2/R–TiO_2/M.

Table 1. Thickness of layers of the samples studied

Sample	TiO_2 layer	$CH_3NH_3PbI_3$
TiO_2/C–$CH_3NH_3PbI_3$	100 nm	400 nm
TiO_2/R–$CH_3NH_3PbI_3$	600 nm	600 nm
TiO_2/M–$CH_3NH_3PbI_3$	500 nm	600 nm

Some luminescent properties of perovskites are listed in Table 2. Parameter I_{max}/D_{470} (I_{max} is the maximum luminescence intensity and D_{470} is the optical density of the perovskite film at $\lambda_{reg} = 470$ ns) makes it possible to determine the quality of the films synthesized. Films with a high defect concentration exhibit a less intense photoluminescence [14]. For comparison,

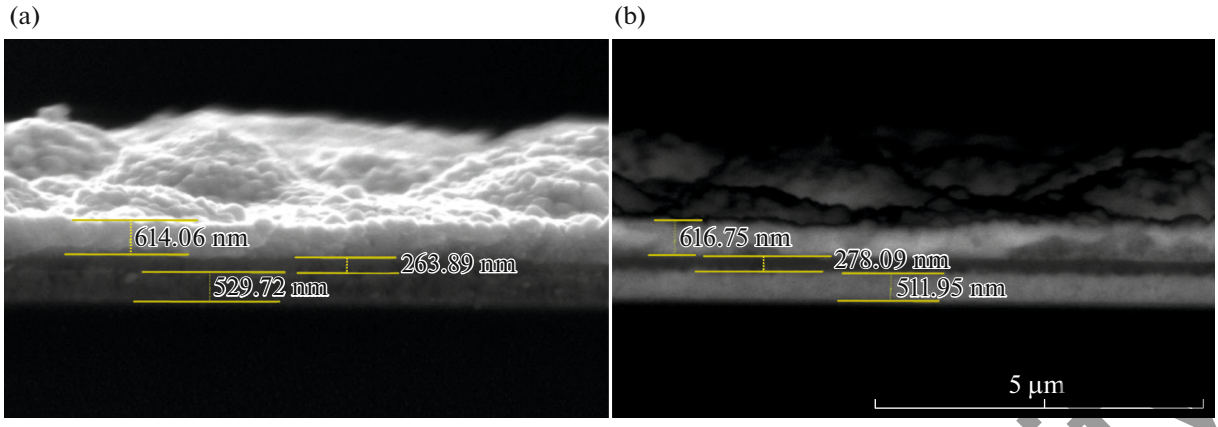

Fig. 3. Cross sections of a TiO_2/M–$CH_3NH_3PbI_3$ film obtained using (a) secondary and (b) backscattered electron detectors.

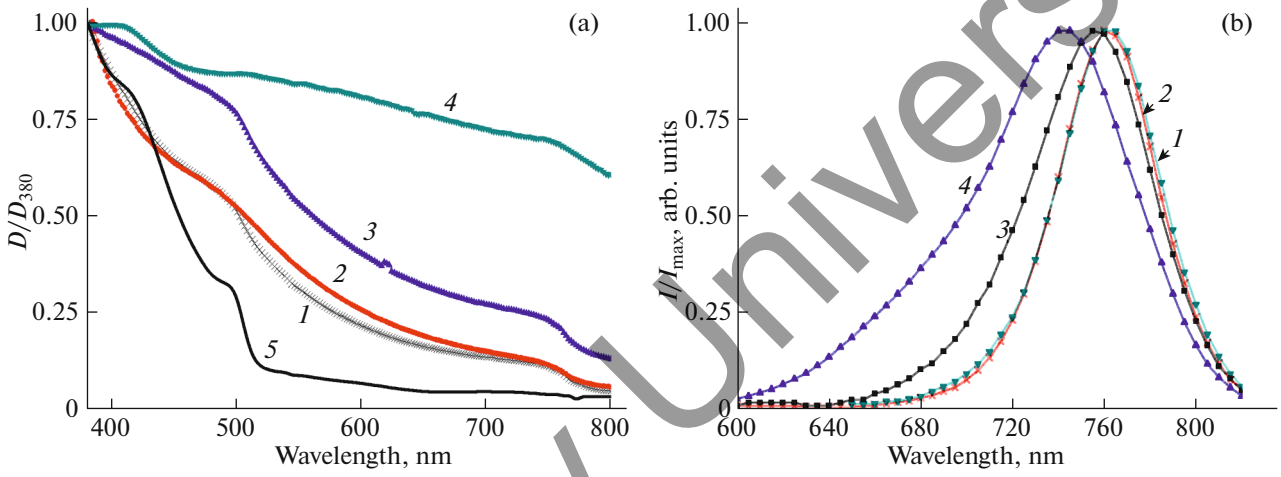

Fig. 4. (a) Absorption and (b) luminescence spectra of $CH_3NH_3PbI_3$ films synthesized on the (*1*) FTO, (*2*) TiO_2/C, (*3*) TiO_2/R, and (*4*) TiO_2/M surfaces, as well as (*5*) absorption spectrum of a PbI_2 film.

Table 2 also presents data for a perovskite film on the FTO surface. The obtained data indicate that the defect concentration is higher for perovskite films on FTO. The ratio I_{max}/D_{470} is almost identical for all films, which means that the perovskite films formed on TiO_2 with different surface morphologies have similar quality.

Table 2. Influence of the TiO_2 film properties on the perovskite film luminescence intensity, as well as on the luminescence intensity and lifetime quenching due to deposition of a Spiro-OMeTAD film on perovskite

Sample	I_{max}/D_{470}*	I_1/I_2**	τ_1/τ_2***
FTO–$CH_3NH_3PbI_3$	0.065	15.2	3.19
TiO_2/C–$CH_3NH_3PbI_3$	0.16	4.08	1.08
TiO_2/R–$CH_3NH_3PbI_3$	0.16	3.78	1.10
TiO_2/M–$CH_3NH_3PbI_3$	0.15	1.5	1.64

* D_{470} is the optical density of the perovskite film at λ_{reg} = 470 ns.
** I_1 and I_2 are the perovskite film luminescence intensities before and after deposition of a Spiro-OMeTAD film.
*** τ_1 and τ_2 are the perovskite luminescence lifetimes before and after deposition of Spiro-OMeTAD film.

Information on the time characteristics of charge transfer from the perovskite film to layers with the *n*–*p*-type conductivity can be obtained from measurements of the luminescence kinetics of the samples. The luminescence kinetics in the nanosecond range contains the rise and decay stages (Fig. 5). The luminescence rise time (Δt, Fig. 5a) depends on the properties of the surface on which the perovskite film is formed. The longest and shortest luminescence rise times are observed for perovskite on the FTO and mesoporous TiO_2 surfaces, respectively. The luminescence of $MaPbI_3$ on FTO has exponential decay and lifetime τ = 22.3 ns (Table 3, $k = 1/\tau$). This time is close to the value of τ obtained for the $MaPbI_3$ perovskite film on a glass surface [6, 7]. For the $MaPbI_3$ film on the surface of TiO_2 films, the luminescence

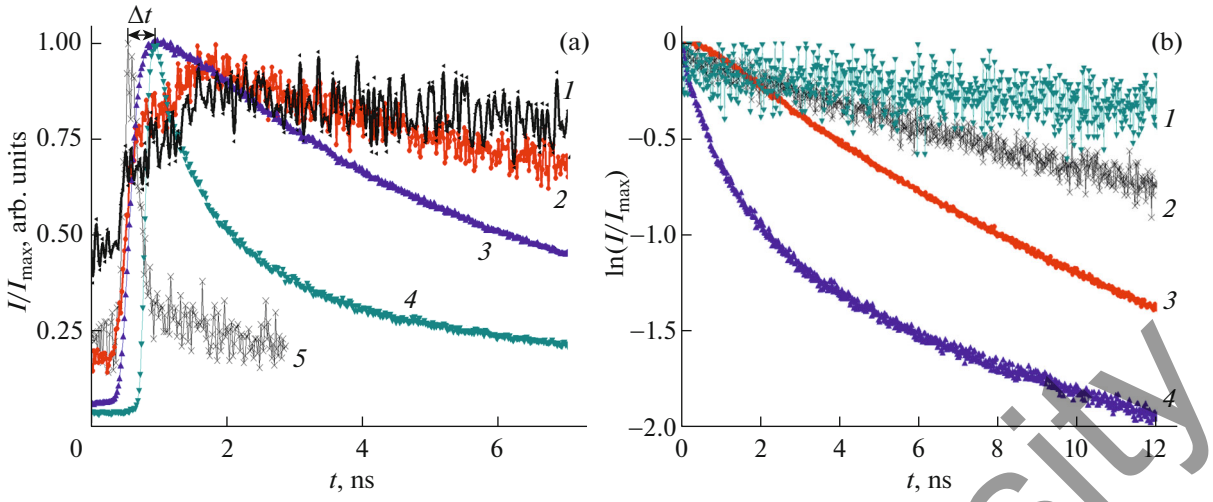

Fig. 5. Luminescence kinetics of perovskite films on (a) linear and (b) logarithmic scales for samples (*1*) FTO–$MaPbI_3$; (*2*) TiO_2/C–$MaPbI_3$, (*3*) TiO_2/R–$MaPbI_3$, and (*4*) TiO_2/M–$MaPbI_3$. Curve (*5*) corresponds to the laser pulse.

lifetime decreases and the charge transfer rate k increases (Table 3).

We can suggest that the existence of the rise and decay stages of the luminescence kinetics (Fig. 5a, curves *1–4*) is related to generation of charge carriers and their subsequent recombination in the perovskite film. The decrease in the time delay Δt between the laser pulse and the beginning of the luminescence decay for $MaPbI_3$ on the rough and mesoporous TiO_2 surfaces can be related to an increase in the concentration of defects in the film or to a decrease in the time needed for charge carriers to reach a recombination center. However, comparison of the ratio I_{max}/D_{470} for perovskite films formed on different TiO_2 surfaces shows its identity. This allows us to conclude that the defect concentrations in perovskite films on different TiO_2 surfaces are close to each other. Therefore, the main reason for the decrease in the luminescence delay for $MaPbI_3$ on TiO_2 surfaces can be related to a decrease in the time for which charge carriers reach recombination centers.

Table 3. Time characteristics of charge carrier extraction from perovskite films

Sample	k_1, ns^{-1}*	k_2, ns^{-1}**	Δt, ns***
FTO–$CH_3NH_3PbI_3$	0.045	0.098	1.53
TiO_2/C–$CH_3NH_3PbI_3$	0.043	0.004	1.20
TiO_2/R–$CH_3NH_3PbI_3$	0.139	0.015	0.49
TiO_2/M–$CH_3NH_3PbI_3$	0.165	0.106	0.47

* Rate constant of electron transfer from perovskite to titania film, $k_1 = 1/\tau$.

** Rate constant of transfer from perovskite to Spiro-OMeTAD determined as $k_2 = k_{MaPbI_3–Spiro–OMeTAD} - k_{MaPbI_3}$, where k_{MaPbI_3} and $k_{MaPbI_3–Spiro–OMeTAD}$ are the charge carrier transfer constants determined for the samples of perovskite films before and after deposition of a Spiro-OMeTAD film.

*** Time of luminescence intensity rise after laser excitation. Δt is determined as shown in Fig. 5a.

Parameters I_1/I_2 and τ_1/τ_2 (Table 2) allow one to estimate the efficiency of hole transfer from perovskite into the Spiro-OMeTAD layer and implicitly estimate the efficiency of electron transfer from the perovskite film into the film with electron conductivity (TiO_2). Comparison of parameters I_1/I_2 and τ_1/τ_2 shows that electron transfer is most efficient in the TiO_2/M–$MaPbI_3$ sample. The transfer of holes is most efficient in the FTO–$MaPbI_3$ sample.

The luminescence lifetime decreases for $MaPbI_3$ films on the surface of TiO_2 films (Table 3). As is known [6], the charge transfer efficiency can be estimated by quenching of the luminescence intensity or lifetime. The luminescence decay kinetics of samples TiO_2/C–$MaPbI_3$ and TiO_2/R–$MaPbI_3$ is exponential (Fig. 5b). The luminescence decay kinetics of the TiO_2/M–$MaPbI_3$ sample is nonexponential (Fig. 5b). In addition, in contrast to the other samples, the shape of the luminescence decay curve for the TiO_2/M–$MaPbI_3$ sample depends on the recording wavelength. As the recording wavelength decreases from 800 to 730 nm, τ decreases from 6.07 to 0.54 ns. This dependence can be related to the influence of defects of the mesoporous TiO_2 film and the energy characteristics of generated charge carriers on the efficiency of electron extraction from the perovskite film. The shorter lifetime indicates a higher rate of high-energy electron transfer from perovskite to TiO_2.

Analysis of the data given in Table 3 shows that the best electron transfer occurs in the TiO_2/M–$MaPbI_3$

system. A high k_2 is observed for the FTO–$MaPbI_3$ sample. With addition of Spiro-OMeTAD, the luminescence lifetime for $MaPbI_3$ on the TiO_2/C surface decreases insignificantly, no more than by 1.5 times. These results show that a strong decrease in the luminescence lifetime after deposition of a Spiro-OMeTAD film can be observed for samples with a low rate of charge transfer from the perovskite film to the oxide semiconductor. An exception is the sample based on TiO_2/M.

Additional information on the dynamics of spin-correlated charge carriers in perovskite films can be obtained by studying the influence of an external MF on the perovskite luminescence kinetics. For this purpose, we measured the luminescence kinetics of perovskites on the TiO_2/C and TiO_2/M surfaces in a MF. The measurements revealed a weak dependence of the magnetic effect (ME) on the signal recording time for the sample on the TiO_2/C surface (Fig. 6, curve *3*). These dependence only slightly changes after deposition of a Spiro-OMeTAD film on perovskite.

In contrast to the TiO_2/C–$MaPbI_3$ sample, the TiO_2/M–$MaPbI_3$ sample exhibits a time-dependent ME. The ME in this case is much stronger than the ME observed in [7, 9]. As is shown in [9], the influence of an external MF on the photoluminescence of perovskite films is related to the Δg mechanism. Based on the formula given in [9]

$$\omega = \frac{1}{T} = \frac{\mu_B \Delta g B}{\hbar}, \quad (1)$$

where μ_B is the Bohr magneton, Δg is the difference between the g-factors in the perovskite film ($\Delta g \sim 0.65$ [9]), and B in the MF induction, it is possible to estimate the frequency ω and the oscillation period of electron–hole pairs in perovskite, which are related to the difference between the g-factors of charge carriers in the pair. The oscillation period was estimated to be $T \sim 35 \times 10^{-12}$ s. This value is considerably higher than the time characteristics obtained by us for ME and lower than the exciting laser pulse duration ($\tau = 120 \times 10^{-12}$ s). Because of this, oscillations of the spin state of electron–hole pairs formed in the perovskite film cannot be detected under our experimental conditions. Thus, the observed time dependence of the ME is related to the existence of additional magneto-sensitive processes in perovskite films upon their photoexcitation.

For the ME in TiO_2/M–$MaPbI_3$ observed in a nanosecond time range, the delay between the laser pulse termination and the ME maximum is measured to be 2.2 ns (Fig. 6). This time delay differs from Δt given in Fig. 5a. Using the diffusion coefficients ($D_n = 0.18$ cm^2/s, $D_p = 2.3$ cm^2/s) for $MaPbI_3$ films 390 nm thick obtained in [17], we estimated the diffusion lengths for electrons and holes in $MaPbI_3$. These lengths at $t = 2.2$ ns were found to be $L_{D(n)} = 200$ nm and $L_{D(p)} = 700$ nm. Comparing these parameters with the size of the $MaPbI_3$ film crystallites (100–200 nm), we can conclude that the main contribution to the ME time dependence $g(B)$ is made by electrons reached the crystallite boundary.

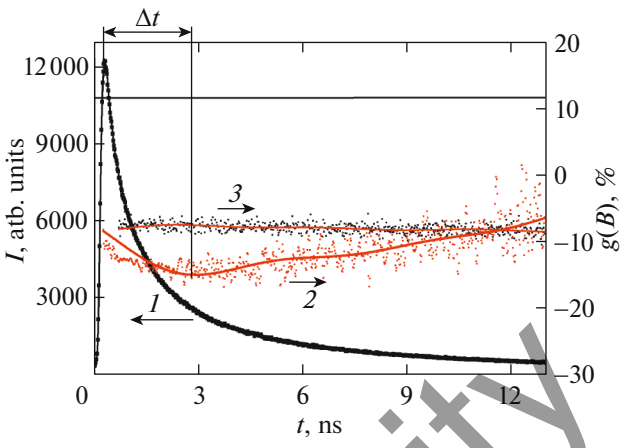

Fig. 6. (*1*) Luminescence kinetics of the perovskite film in the TiO_2/M–$MaPbI_3$ sample and (*2*, *3*) time dependences of magnetic effect $g(B)$ for samples (*2*) TiO_2/M–$MaPbI_3$ and (*3*) TiO_2/C–$MaPbI_3$. $B = 0.5$ T.

Thus, we can suppose that the time dependence of the ME is related to the recombination luminescence caused by the forward and backward electron transfer between perovskite and TiO_2. The recombination nature of the luminescence in the TiO_2/M–$MaPbI_3$ system is confirmed by the fact that the luminescence decay curve can be described within the empirical Becquerel equation [18, 19]. Comparison showed that the luminescence kinetics in the range from 5 to 20 ns after excitation is, with a 0.98 accuracy, described by the dependence

$$\frac{1}{\sqrt{I/I_0}} = 1 + k_{ef}t, \quad (2)$$

where k_{ef} is the effective luminescence decay rate constant of the film. The constant k_{ef} for the TiO_2/M–$MaPbI_3$ sample is 2.3×10^6 s^{-1} (accuracy 0.98). Comparison of constants k_{ef} revealed that the recombination rate in the TiO_2/M–$MaPbI_3$ sample is higher than in the other samples.

The existence of the spectral dependence of the lifetime and the time-dependent ME indicate a complex character of the ME formation in the TiO_2/M–$MaPbI_3$ sample. This also testifies to the presence of a large fraction of recombination luminescence in the observed emission. The spectral dependence of the perovskite luminescence lifetime in the TiO_2/M–$MaPbI_3$ sample allows us to suggest that electron migration in the porous TiO_2 film occurs with participation of shallow defect levels in TiO_2 [20].

CONCLUSIONS

We have studied the luminescent properties of $CH_3NH_3PbI_3$ perovskite films synthesized on the surfaces of TiO_2 films with different morphologies. The $CH_3NH_3PbI_3$ luminescence intensity and lifetime decrease in samples with TiO_2 and Spiro-OMeTAD, which is related to charge transfer from perovskite to the layers with the *n*- and *p*-type conductivity. The luminescence decay kinetics of samples TiO_2/C–$MaPbI_3$ is exponential, which indicates a small contribution of recombination luminescence to the perovskite film luminescence. The luminescence kinetics in the TiO_2/M–$MaPbI_3$ sample depends on the recording wavelength. As the wavelength decreases from 800 to 730 nm, the luminescence lifetime decreases from 6.07 to 0.54 ns. This dependence testifies to migration of electrons injected from the perovskite film over defect levels in TiO_2. The time dependence of the ME on the luminescence kinetics of perovskite on the surface of the mesoporous semiconductor film is related to the recombination luminescence caused by the forward and backward electron transfer between perovskite and TiO_2.

FUNDING

This work was supported by the Ministry of Education and Science of the Republic of Kazakhstan (grant no. BR05236691).

REFERENCES

1. B. O'Regan and M. Gratzel, Nature (London, U.K.) **353**, 737 (1991).
2. B. Kraabel, C. H. Lee, D. Mcbranch, et al., Chem. Phys. Lett. **213**, 389 (1993). https://doi.org/10.1016/j.cplett.2013.08.049
3. A. Kojima, K. Teshima, Y. Shirai, and T. Miyasaka, J. Am. Chem. Soc. **131**, 6050 (2009). https://doi.org/10.1021/ja809598r
4. Best Research-Cell Efficiency Chart. https://www.nrel.gov/pv/cell-efficiency.html.
5. W. Peng, B. Anand, L. Liu, S. Sampat, B. Bearden, A. V. Malko, and J. Yves, Nanoscale **8**, 1627 (2016). https://doi.org/10.1039/c5nr06222e
6. K. Pydzińska, J. Karolczak, I. Kosta, et al., ChemSusChem **9**, 1 (2016). https://doi.org/10.1002/cssc.201600210
7. Q. Zhang, H. Yu, F. Zhao, L. Pei, J. Li, K. Wang, and B. Hu, Adv. Funct. Mater., 1904046 (2019). https://doi.org/10.1002/adfm.201904046
8. H. Xu, M. Wang, Z. Yu, K. Wang, and B. Hu, Adv. Phys. **68**, 49 (2019). https://doi.org/10.1080/00018732.2019.1590295
9. C. Zhang, D. Sun, C. X. Sheng, Y. X. Zhai, K. Mielczarek, A. Zakhidov, and Z. V. Vardeny, Nat. Phys. **11**, 427 (2015). https://doi.org/10.1038/nphys3277
10. F. Zheng, L. Z. Tan, S. Liu, and A. M. Rappe, Nano Lett. **15**, 7794 (2015). https://doi.org/10.1021/acs.nanolett.5b01854
11. V. V. Belykh, D. R. Yakovlev, M. M. Glazov, Ph. S. Grigoryev, M. Hussain, J. Rautert, D. N. Dirin, M. V. Kovalenko, and M. Bayer, Nat. Commun. **10**, 673 (2019). https://doi.org/10.1038/s41467-019-08625-z
12. O. Gunawan, S. R. Pae, D. M. Bishop, et al., Nature (London, U.K.) **575**, 151 (2019). https://doi.org/10.1038/s41586-019-1632-2
13. T. M. Serikov, N. Kh. Ibrayev, and G. S. Amanzholova, Euras. Phys. Tech. J. **13**, 60 (2016).
14. D. A. Afanasyev, K. Yu. Mirzoev, and N. Kh. Ibrayev, IOP Conf. Ser.: Mater. Sci. Eng. **289**, 012001 (2018). https://doi.org/10.1088/1757-899X/289/1/012001
15. A. Dualeh, T. Moehl, N. Tétreault, J. Teuscher, P. Gao, M. Kh. Nazeeruddin, and M. Grätzel, J. Am. Shem. Soc. **8**, 362 (2014). https://doi.org/10.1021/nn404323g
16. D. A. Afanasyev, N. Kh. Ibrayev, A. K. Nurmakhanova, and M. G. Kucherenko, Opt. Spectrosc. **124**, 789 (2018). https://doi.org/10.1134/S0030400X18060024
17. Y. Li, W. Yan, Y. Li, et al., Sci. Rep. **5**, 14485 (2015). https://doi.org/10.1038/srep14485
18. V. A. Antipin, S. L. Khursan, R. R. Kinzyabulatov, and Yu. A. Lebedev, Vestn. Bashkir. Univ. **19**, 1156 (2014).
19. V. Pagonis, H. Phan, R. Goodnow, S. Rosenfeld, and P. Morthekai, J. Lumin. **154**, 362 (2014). https://doi.org/10.1016/j.jlumin.2014.05.008
20. X. Wang, Zh. Feng, and J. Shi, Phys. Chem. Chem. Phys. **12**, 7083 (2010). https://doi.org/10.1039/b925277k

Translated by M. Basieva